

See discussions, stats, and author profiles for this publication at: <https://www.researchgate.net/publication/286457801>

# An On-Board Wireless Multi-Sensor Measurement System for Rotating Turbomachinery Application

Conference Paper · November 2015

CITATIONS

0

READS

143

4 authors, including:



**Michel Mansour**

Limmat Scientific AG

25 PUBLICATIONS 122 CITATIONS

[SEE PROFILE](#)



**Anestis Kalfas**

Aristotle University of Thessaloniki

128 PUBLICATIONS 733 CITATIONS

[SEE PROFILE](#)

Some of the authors of this publication are also working on these related projects:



Future Energy Research Profile (KKS) [View project](#)



Study of High Temperature Supercritical CO2 Power Generation Cycles [View project](#)

# An On-Board Wireless Multi-Sensor Measurement System for Rotating Turbomachinery Application

Michel Mansour<sup>1</sup> Patrick Rebholtz<sup>1</sup> Anestis Kalfas<sup>2</sup> Reza S. Abhari<sup>1</sup>

<sup>1</sup>Laboratory for Energy Conversion, Department of Mechanical and Process Engineering, ETH Zurich, Switzerland

<sup>2</sup>Department of Mechanical Engineering, Aristotle University of Thessaloniki, 54124 Thessaloniki, Greece

## ABSTRACT

A novel multi-sensor wireless measurement system for measurements in the rotating frame of reference is presented and demonstrated in this paper. The system is comprised of newly developed in-house surface mount pressure sensors and wireless signal conditioning and acquisition boards. The surface mount pressure sensor assemblies are packaged a miniature aluminum casing of 1.75mm x 0.81 x 0.47mm. The RTV-coated assembly offers the highest measurement bandwidth of 210 kHz which provides a measurement bandwidth at least 40 times above the maximum intended blade passing period. The uncertainty analysis performed shows that the pressure sensors offer a measurement accuracy of  $\pm 87\text{Pa}$  and  $\pm 77\text{Pa}$  in absolute and fluctuating pressure measurements, respectively. The sensors and the wireless data acquisition boards provide a high signal-to-noise ratio with a pressure resolution of 6Pa on the raw signal. The measurement system is successfully deployed in an axial one-and-1/2-stage-turbine facility, and preliminary measurements are presented and discussed.

## NOMENCLATURE

A	area	[m <sup>2</sup> ]
L	length	[m]
P,p	pressure	[Pa]
S	sensitivity	[mV/mbar]
T	temperature	[°C]
U	pressure signal	[V]
U <sub>e</sub>	Temperature signal	[V]
f	frequency	[Hz]
k	stiffness	[Nm/rad]
m	mass	[kg]

## Greek

$\sigma$	standard deviation
----------	--------------------

## Abbreviations

FRAP	fast-response aerodynamic probe
TCO	temperature coefficient of offset
TCS	Temperature coefficient of span
SMA-RTV	surface mount pressure sensor assemblies

SMA-PS

coated with RTV  
surface mount pressure sensor assemblies with perforated screen

## Subscripts

abs	absolute
e	excitation
fluct	fluctuating
avg	average value
min	minimum
max	maximum
rel	relative

## INTRODUCTION

In turbomachinery, blades suffer from flutter or forced response depending on the type of application and operating conditions. In the early stage of new turbine or compressor development, the design focuses on satisfying the mechanical integrity of the rotating parts to meet the requirements in terms of expected effective operating hours. For now many years the design of new aero-engines is focusing in minimizing the weight. This is achieved by reducing the number of stages and therefore increasing the blades loading. As reported in [1-3], it is vitally important to study the sources of inter-blade row interactions on the aerodynamic blade excitation to mitigate the risk of early failure. Similarly, centrifugal compressors have gone through considerable developments over the past 10 years, evolving towards high speed, high efficiency and high pressure ratio compressors. The current design trends tend to increase the risks of failure. Several research groups have worked in identifying the sources of excitations related to wake potential field interaction with the impeller as well as with the primary and secondary flow paths [4-6].

This process relies on the capability to predict the cause and magnitude of blade excitation and to assess damping mechanisms. To enable this kind of quantification, the measurement of the unsteady pressure acting of the blades has to be coupled to the blade mechanical deformation over the entire range of intended operating conditions. It requires conducting measurement in the rotating frame of reference, which is more challenging to construct and instrument at the same degree than stationary experiments. This becomes especially true if the blades have to be equipped with a high

number of sensors to ensure a high-measurement density and spatial resolution. Established traditional methods like slip rings are widely used but have shown their practical limits in the quantity and quality of the transferable signals. Wireless transmission techniques with fully integrated surface-mounted pressure sensors have been developed over a decade now, but their usage has remained limited.

The laboratory for Energy Conversion of the Swiss Federal Institute of Technology has a longstanding expertise in developing fast-response instrumentation dedicated to turbomachinery, especially in the field of fast-response aerodynamic probes [7-9], instrumented rotating experiments [5, 10] and fast-pressure sensing [11]. In this paper, the development and performance of a new wireless multi-sensor measurement system for rotating turbomachinery application, with a special focus on the newly developed surface fast-pressure sensor, is presented. Then, some preliminary results measured with the newly developed system in one-and 1/2-stage unshrouded high work turbine are presented and discussed.

### Surface-mounted fast-pressure sensors

The principal requirements for the surface mount pressure transducers is the capability to resolve the unsteady pressure fluctuations along the blade chord of both LEC's research axial turbine rotor blades and radial compressor. The radial compressor application sets most of the design requirements such as a maximum packaging thickness of less than a millimeter due to the reduced impeller blade thickness close to the tip. The measurement bandwidth is set to be at least 10 harmonics above the maximum blade passing frequency of 5KHz, whereas the sensor assemblies have to be able to withstand steady centrifugal acceleration of  $2 \cdot 10^6 \text{ m/s}^2$ . On the other hand the signal-to-noise ratio should allow resolving surface pressure variation down to at least 0.1mbar in order to study the sources and magnitude of blade unsteady loading.

### Sensor Packaging

The sensing elements of the surface mounted pressure transducers, Fig. 1, employ a miniature pressure absolute sensor die. This sensor is one of the smallest absolute pressure die available in the market with cross section dimensions of  $300 \times 180 \mu\text{m}$  and a length of 0.9mm, which makes it particularly prone for achieving a small packaged assembly with high measurement bandwidth characteristics.

The packaging and bonding techniques that were used ensure optimal spatial resolution, measurement bandwidth and protection of the sensors in harsh conditions. Moreover the present design provides a high degree of reliability and low levels of thermal disturbance to the sensors as the probe can experience large temperature and pressure fluctuations.



**Fig. 1 Surface mount pressure sensor photograph**

As shown in Fig. 2, in the context of the presented work two different assemblies were designed and assessed. In both cases the absolute piezo-resistive chip is glued onto a miniature aluminum casing of 1.75mm x 0.81 x 0.47mm.

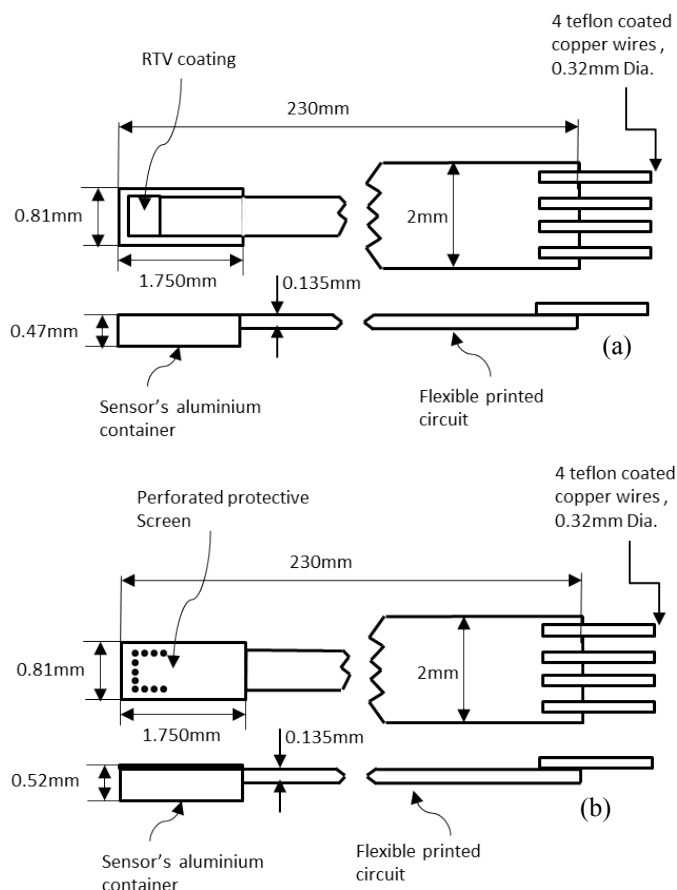


**Fig. 2: (a) Surface mount pressure transducer assembly with RTV coating (SMA-RTV), (b) surface mount pressure transducer assembly with perforated screen (SMA-PS)**

The achieved miniature dimensions allow the sensor installation on impeller blades with a thickness of a few millimeters. The sensors are installed in their aluminium casing using a silicone RTV with very low E-modulus. The glue is based on an inorganic ground structure, which offers large temperature range of operation ( $-90 - 200^\circ\text{C}$ ) and is highly resistant to corrosive media. Thus the thermo-mechanical stresses are minimized once the container is installed onto the test surface. The sensor is connected to the acquisition system through a flexible printed circuit of 0.135mm in thickness, reducing its interaction with the flow boundary layer. As shown in Fig. 2 (a), the first surface mount sensor assembly named SMA-RTV is coated with a

layer of hydrophobic RTV, which enables the operation of the sensor in water or in wet steam. Whereas the second assembly called SMA-PS, Fig. 2 (b), has a protective cover placed on top of the sensor for operation in harsh and particle laden flows. The perforated screen consists of a 0.05mm thick aluminum sheet with 11 pressure holes of 0.08mm in diameter. The cover is placed 0.150mm above the uncoated sensor diaphragm and has a thickness of 0.05mm, generating a small volume of air between the perforated holes and the sensor's diaphragm.

### Static calibration

Both absolute pressure sensor assemblies are calibrated in a fully automated and temperature controlled pressure chamber. The pressure chamber is equipped with high a precision differential pressure controller, DPI 520, which has a range of -1 to +1bar relative to the atmospheric, and with an absolute pressure transducer Keller PA-33X. These two transducers are used to control and measure the applied absolute pressure onto the sensor assemblies. The sensors were calibrated over a pressure and temperature range of 300-1800mbar and 15-95°C, respectively. It should be noted that the sensors were calibrated in a constant current mode, which reduces the pressure sensitivity dependency to temperature compared to an operation in constant voltage mode. In addition to that the constant current mode makes the excitation voltage  $U_e$  sensitive to temperature. Table 1 summarizes the main characteristics of both assemblies SMA-RTV and SMA-PS, the sensor averaged characteristics were derived over the calibration of 10 assemblies of each type. In general, despite the difference in sensor packaging described in the sensor assembly section both assemblies show very similar average static calibration characteristics. Both assemblies exhibit a pressure sensitivity close to -3.2 mV/mbar \*mA with less than 6% variation in sensitivity over a set of ten assemblies that were tested. When looking at the temperature coefficient of offset, as defined in Eq. 1, which is the measure of the pressure signal offset variation sensitivity to temperature range as plotted in Fig. 3(b). Again both assemblies end up with very similar values of around 10.5 mV/K mA, which around 0.27% of the full scale output.

$$TCO = \frac{U(T_{max}, p_{min}) - U(T_{min}, p_{min})}{(T_{max} - T_{min})} \quad \text{Eq. 1}$$

The third quantified sensor static characteristic is the temperature coefficient of span, as shown in Eq. 2. This parameter quantifies the dependency of the pressure sensitivity over the temperature range of calibration as plotted in Fig. 3(a). Due to the operation in constant current mode this quantity shows a very low dependency of less 0.074% per degree kelvin for both assemblies. This is a key feature insuring a high degree of accuracy in the measured fluctuating pressure over the entire temperature range of operation.

$$TCS = \frac{1}{S(T_{mean})} \frac{S(T_{max}) - S(T_{min})}{(T_{max} - T_{min})} \quad \text{Eq. 2}$$

**Table 1: Pressure transducers static calibration properties**

properties	SMA-RTV	SMA-PS
Pressure sensitivity: S [mV/mbar], $\sigma_s$ @ 25°C	$-3.18 \pm 0.19$	$-3.15 \pm 0.18$
Temperature coefficient of offset: TCO [mV/K mA], $\sigma_{TCO}$ @ p = 300mbar	$10.37 \pm 0.19$	$10.89 \pm 0.19$
Temperature coefficient of Span: TCS [1/K], $\sigma_{TCS}$	$-7.3 \cdot 10^{-4} \pm 2 \cdot 10^{-5}$	$-7.4 \cdot 10^{-4} \pm 1.9 \cdot 10^{-5}$

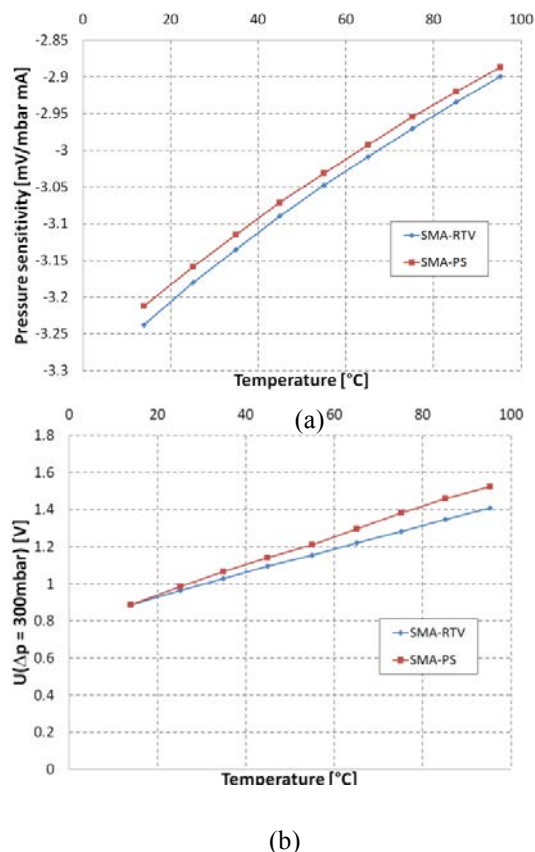


**Fig. 3: (a) pressure sensitivity versus applied temperature, (b) zero pressure offset versus temperature.**

In order to account for the temperature dependency of the sensor pressure output, the sensors must be calibrated over the full range of intended temperature use and the pressure and temperature. During that procedure both the pressure signal  $U$  and temperature signal  $U_e$  were acquired as shown in Fig. 4(a) and (b). For the measurements, a fifth-order polynomial interpolation, Eq. 1 and Eq. 2 is then used to determine the pressure and temperature from the measured sensor signals. Fig. 4(c) and (d) show the pressure and temperature models deviations over the full range of calibration. The polynomial interpolation models have on an average an absolute deviation of 30pa and 0.09°C, respectively.

$$p(U, U_e) = \sum_{i=0}^m \sum_{j=0}^n K_{p_{i,j}} U^i U_e^j \quad \text{Eq. 3}$$

$$T(U, U_e) = \sum_{i=0}^m \sum_{j=0}^n K_{T_{i,j}} U^i U_e^j \quad \text{Eq. 4}$$

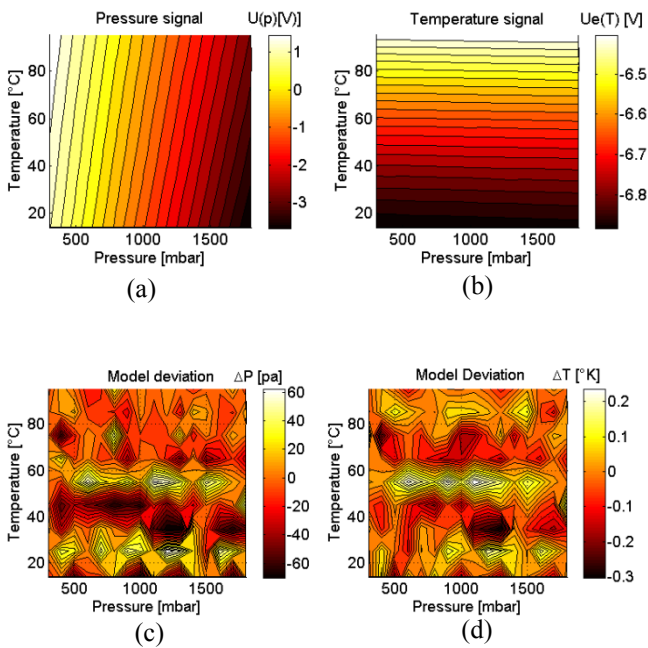


**Fig. 4: Sensor calibration model: (a) pressure signal voltage  $U(p)$  as function of pressure and temperature, (b) sensor temperature signal voltage as a function of applied pressure and temperature, (c) pressure calibration model quality, (d) temperature calibration model quality**

### Dynamic Calibration

The dynamic responses of the surface mount pressure transducers are determined using an in-house gas dynamic low-pressure shock tube. As shown in Fig. 5, the shock tube facility consists of a 50mm diameter pipe that has a total length of 5 meter. The test section is located 600mm upstream of a bursting diaphragm, generating a 800mbar pressure step. A fast-pressure sensor, located 200mm away from the diaphragm, detects the pressure wave and triggers the simultaneous acquisition of the surface mount pressure sensor and of the reference pressure sensor, respectively. The signals are acquired at sampling rate of 1.6MHz with a resolution of 12bit. The goal of the dynamic calibration is to determine the transfer function of both assemblies and their respective measurement bandwidth. By modeling the pressure sensor output as a linear and time invariant system, the transfer function can also be used to correct the pressure signal until second harmonic of the sensor eigenfrequency.

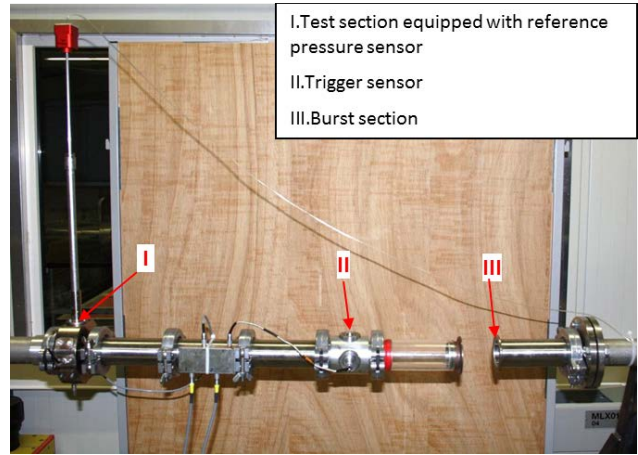


**Fig. 5: Shock tube arrangement**

The low-pressure side of the shock tube, where test section is located, is evacuated until the rupture of the thin diaphragm occurs. The shockwave travels from the ambient high-pressure side to the low-pressure side. The generated pressure step is measured at the same plane by an in-house uncoated flush mounted reference sensor as shown in Fig. 6.

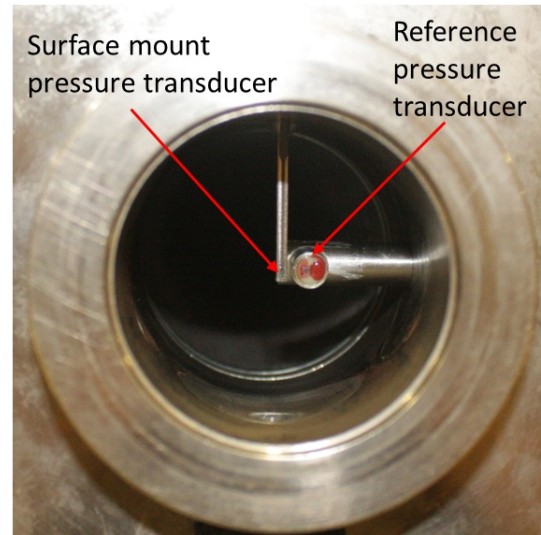


**Fig. 6: Close up view of the shock tube test section equipped with the surface mount pressure transducer and the reference pressure transducer.**

Fig. 7 shows the typical set of measured pressure signals used for the determination of the surface mount pressure sensor assemblies' transfer function. Only the first 10ms are used for data analysis in order to avoid processing part of the signal that is affected by reflection waves traveling backward in the shock tube assembly.

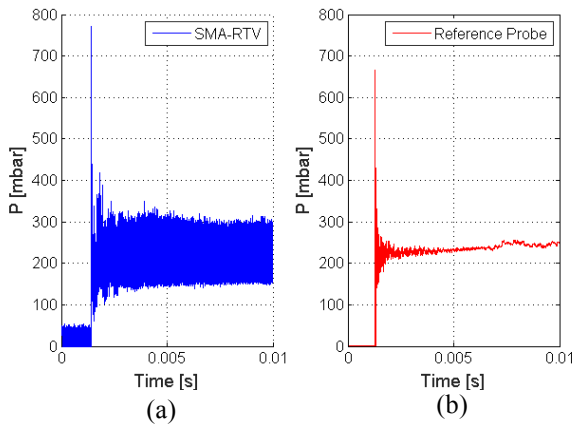


**Fig. 7: typical measured pressure signal of (a) SMA-RTV sensor and (b) reference sensor used for the determination of the SMA-RTV's transfer function**

Fig. 8(a) shows the amplitude frequency spectrum of the SMA-RTV assembly as well as the reference pressure sensor up to a frequency of 600kHz. The peak present at 520kHz is related to eigenfrequency of the reference pressure sensor's membrane which is not coated with RTV. Whereas, the peak present at 229kHz and its harmonic at 458kHz are related the surface mount pressure sensor's membrane eigenfrequency. Its eigenfrequency has dropped due to the presence of the RTV coating, increasing the apparent sensor membrane weight. As shown in Eq.5 the added mass of RTV will reduce linearly the membrane eigenfrequency. The transfer function is computed as the quotient of both the cross power spectral density of the probe and reference signal, and the power spectral density of the reference signal. The amplitude of the transfer function is plotted in for a frequency range from 10 to 600 kHz. Results are averaged over five measurements in order to account for the imperfect burst of the shock tube diaphragm. As shown in Fig. 8(b), The resulting SMA-RTV transfer shows an amplification of the pressure signal of +3dB at 210kHz, which sets the natural measurement bandwidth of SMA-RTV assemblies. This result is in line with the measurement bandwidth reported by Rollinger et al. [11] on a similar type assembly with the similar amount of applied RTV coating

$$f = \frac{1}{2\pi} \sqrt{\frac{k}{m}} \quad \text{Eq. 5}$$

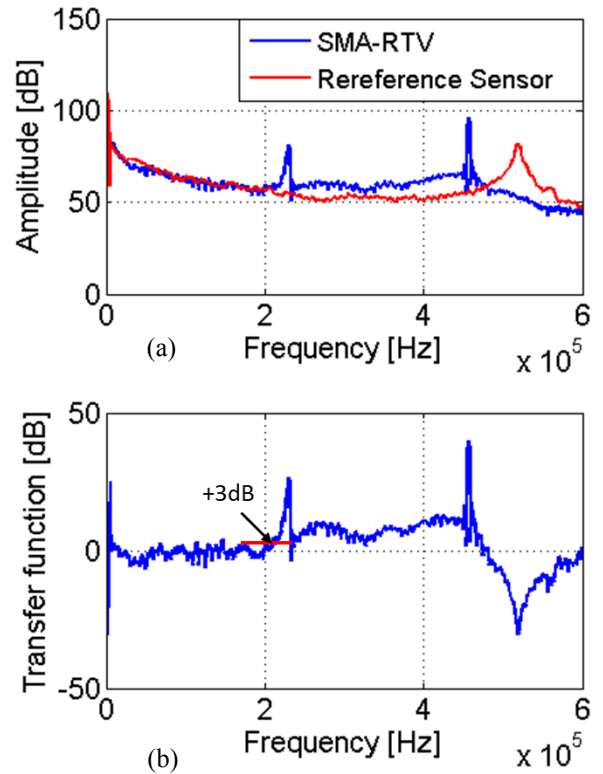


**Fig. 8: (a) amplitude frequency response of the SMA-RTV pressure sensor and of the reference pressure sensor, (b) SMA-RTV pressure sensor transfer function**

On the other hand Fig. 9 (a) shows the amplitude frequency response of the surface mount pressure sensor equipped with a perforated cover. The pneumatic cavity between the perforated screen and the piezo-resistive sensor membrane can influence the unsteady pressure measurements. The acoustic resonance is associated with the length and the volume of the pneumatic cavity, as shown in the Helmholtz resonator expression in Eq. 6 , which implies that the measured signals around the eigenfrequency of the pneumatic cavity are strongly amplified and have a phase shift [12]. It can be seen that the amplitude of the SMA-PS sensor assembly starts deviating from the reference pressure sensor already around 50kHz. As seen in Fig. 9 (b), the amplitude is flat up to a frequency of 51kHz, above which the amplitudes are in excess of 3dB. Thus the cutoff frequency of 51kHz determines the bandwidth of the SMA-PS sensor assembly.

$$f = \frac{c}{2\pi} \sqrt{\frac{A}{VL}} \quad \text{Eq. 6}$$

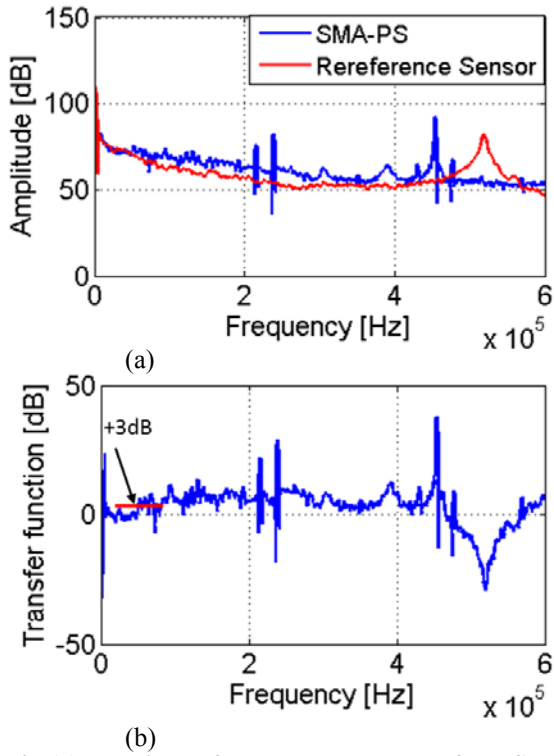


**Fig. 9: (a) amplitude frequency response of the SMA-PS pressure sensor and of the reference pressure sensor, (b) SMA-PS pressure sensor transfer function**

### Uncertainty Analysis

Similar to the analysis conducted by Behr et al. [13], the complete chain of uncertainty sources has been accounted for the calculation of the measured absolute pressure uncertainty. As Shown in Eq. 5, this chain starts with the uncertainties resulting from the pressure transducers used to measure and control the applied absolute pressure onto the sensor assemblies  $\Delta p_{DPI\ 520,rel}$  and

$\Delta p_{Keller,atm}$ , as described in sensor calibration section. The second source of uncertainty comes from the quality of the sensor polynomial calibration model,  $\Delta p_{model}$ . And finally the last source of uncertainty, which is a key quantity to achieve a high accuracy in measured absolute pressure, depends on the measurement uncertainty of the pressure transducer used for the sensor's offset correction used during measurement and called  $\Delta p_{OC}$ . All sources of uncertainty are summarized Table 2. The resulting overall uncertainty in measured absolute pressure of  $\pm 87\text{pa}$  is calculated using the Gaussian error propagation formula and corresponds 0.12% error over the full pressure measurement range. The uncertainty calculation was performed using the GUM Workbench. On the other hand, if the pressure sensors are used to measure only the AC part of the surface pressure signal, the precision on the fluctuating part of the signal,  $\Delta p_{sensor,fluct}$ , is even higher as it does not suffer from the additional source of uncertainty related to the offset correction  $\Delta p_{OC}$ . In this case the uncertainty in measured fluctuating pressure drops to  $\pm 77\text{pa}$  and corresponds to 0.05% error over the full pressure measurement range.

$$\Delta p_{sensor,abs} = \Delta p_{DPI\ 520,rel} + \Delta p_{Keller,atm} + \Delta p_{model} + \Delta p_{OC} \quad \text{Eq. 7}$$

**Table 2: summary of uncertainty sources used for the calculation of the uncertainty in measured absolute pressure and relative pressure**

Quantity	Description	Uncertainty (abs./rel.)
$\Delta p_{DPI\ 520,rel}$	DPI 520 pressure controller	$\pm 50\text{pa} / 0.05\% \text{ FS}$
$\Delta p_{Keller,atm}$	Keller PA-33X atmospheric pressure transducer	$\pm 40\text{pa} / 0.1\% \text{ FS}$
$\Delta p_{model}$	Avg. Calibration model deviation	$\pm 15\text{pa} / 0.02\% \text{ FS}$
$\Delta p_{OC}$	Offset correction prior to measurement	$\pm 50\text{pa} / 0.05\% \text{ FS}$
$\Delta p_{sensor,abs}$	<b>Error in measured absolute pressure (steady + unsteady)</b>	<b><math>\pm 87\text{pa} / 0.12\% \text{ FS}</math></b>
$\Delta p_{sensor,fluct}$	<b>Error in measured fluctuating pressure (unsteady)</b>	<b><math>\pm 77\text{pa} / 0.05\% \text{ FS}</math></b>

### Multi-sensor Wireless data acquisition board

The sensors' voltage signals are acquired using an in-house developed wireless data acquisition boards. The wireless measurement system consists of a fast and high resolution analog-to-digital recorder and logger. They are designed to be operated in the rotating frame of reference up steady accelerations of  $15^{\circ}000\text{ g}$ .

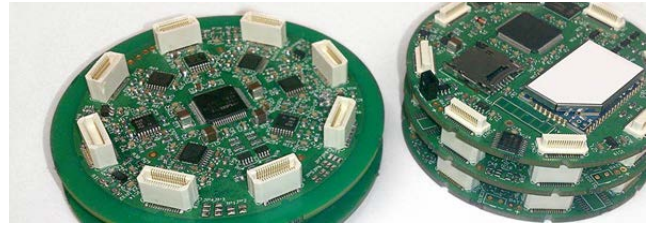


**Fig. 10: Wireless data acquisition board in stacked configuration**

Each boards has 4 analogue input channels synchronized from a single optical signal, and the boards can be stacked up to 4 boards offering 16 simultaneous analogue voltage acquisition channels. Each boards can acquire either 2 piezo-resistive pressure sensors, 4 strain gages or  $Pt_{100}$  operated in a constant current mode. The boards have a diameter and a height of 65mm and 9mm, respectively. The fast-pressure sensors are operated with a constant current of 1mA through individual programmable current sources. The boards are specifically design to acquire dynamic signals up to a sampling frequency of 200kHz per second. The data are temporarily stored on an on-board mini solid state disk, before being sent to an external computer through an embedded Wi-Fi module.

Each acquisition channel is equipped with a dedicated signal conditioning modules with a tunable gain ranging from 1 to 128. For the current application a gain of 128 is used, resulting in a peak-to-peak white noise RMS value of  $160\mu\text{V}$  setting the minimum pressure resolution of approximately 6pa on the measured raw signal; providing a measurement resolution which is an order of magnitude higher than the sensor measurement accuracy.

## Measurement system application and sample results

The SMA-RTV and the wireless data acquisition boards were successfully deployed and operated on the rotor blades of the axial one-and-1/2-stage-turbine facility LISA. As depicted in Fig. 11, the air-loop of the facility is of a quasi-closed type and includes a radial compressor, a two-stage water-to-air heat exchanger and a calibrated venturi nozzle for mass flow measurements. The turbine entry temperature is controlled to an accuracy of 0.3% and the rotor speed is kept constant within  $\pm 0.5 \text{ min}^{-1}$  by the DC generator. The pressure drop across the turbine is stable within 0.3% for a typical measurement. The main parameters of the facility are summarized in Table 1 and more information on the test rig can be found in Behr et al [17].

For the current investigation the turbine test case models a low aspect ratio, highly loaded, high-pressure subsonic aero-engine turbine stage. By-pass air from the compressor is injected through the hub rim seal at the rotor inlet to simulate coolant air that prevents the ingestion of hot flow into the cavity between the stator and rotor disks. The main contributors to the rotor unsteady loading in this configuration are the stator 1 wake and stator 2 potential field as well as the rim seal purge flow. Therefore, in order to decouple the frequencies associated with the inter-blade row interactions, stator 1 and stator 2 were set to a different blade count of 36 and 45 blades, respectively. Which provides a 4/5 vane ratio between stator 1 and 2.

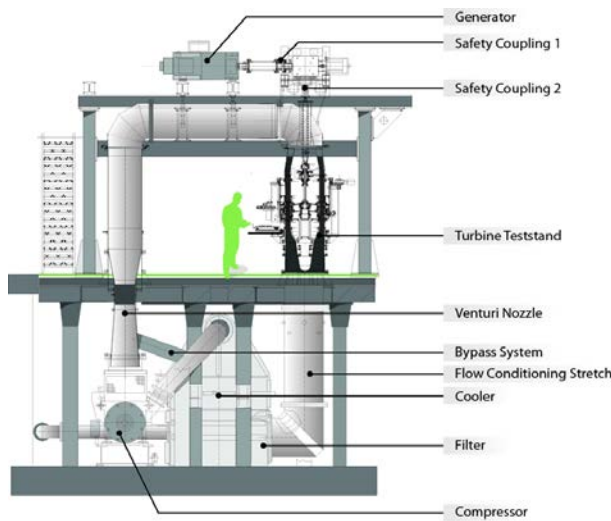


Fig. 11: Schematic of LISA axial turbine experimental facility

Table 3: Main parameters of “LISA” 1.5-stage axial turbine research facility at design operating point

Rotor speed [RPM]	2700
Pressure ratio (1.5-Stage, total-to-static)	1.60
Turbine entry temperature [°C]	55
Total inlet pressure [bar]	1.4
Hub/tip diameter [mm]	660/800
<b>1<sup>st</sup> Stage</b>	
Pressure ratio (1 <sup>st</sup> Stage, total-to-total)	1.35

Degree of reaction [-]	0.39
Loading coefficient [-]	2.36
Flow coefficient [-]	0.65

### Blade count

Stator 1	36
Rotor	54
Stator 2	45

As shown in Fig. 12, 32 SMA-RTV pressure transducer assemblies were installed on the rotor blade at 20% and 85% span. The span locations were specifically selected as they are expected to be regions of highest unsteady loading. In order to minimize the interaction with the flow boundary layer, all pressure transducer assemblies including the flexible printed circuit have been embedded into small grooves machined onto the blade surface. The flexible printed circuits are then brought through the hub platform and the wiring to the acquisition board takes place on the rotor disk. On the other end, the wireless data acquisition and signal conditioning boards were installed on the rotating frame onto the rotor disk at a radial distance of 132mm. In this current work, the unsteady pressure data of sensor S1 and S8, as highlighted in Fig. 12, located on the suction side at 20% span will be shortly discussed. The full data analysis related to the unsteady blade forcing amplitude is presented in Rebholz et al [14].

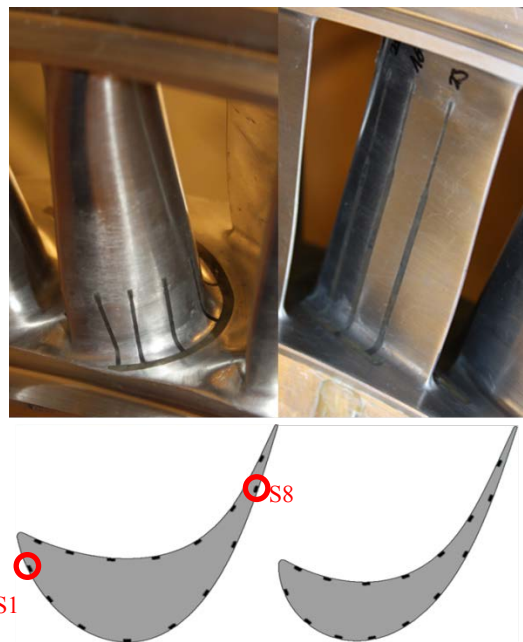
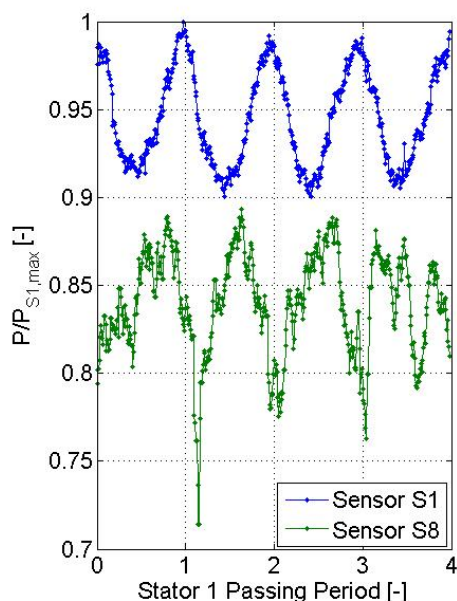


Fig. 12: pictures and schematics of installed pressure sensors at 20% span (right column) and 85% span (left column)

In the current paper, the unsteady pressure data of sensor S1 and S8, as highlighted in Fig. 12, located on the suction side at 20% span will be succinctly analyzed and discussed. The full data analysis related to the unsteady blade forcing amplitude is presented in Rebholz et al [14]. Fig. 13 shows both sensors raw pressure signals non-dimensionalized by the maximum absolute pressure measured by sensor S1 over 4 stator 1 blade passing periods, and Fig. 14 shows their respective frequency spectrum up to 5kHz, non-

dimensionalized by the maximum pressure amplitude measured by sensor S1 at 1620Hz.



**Fig. 13: Pressure fluctuation of Sensor S1 and Sensor S8 located on the suction side at 20% span over four stator 1 vane passing periods**

As it can be seen on Fig. 13, sensor S1 is mainly affected by the periodical impingement of stator 1 vane wake, with four clear periodical peaks in measured fluctuating pressure over four stator 1 vanes passing period. As shown in Fig. 14(a), sensor S1 captures the highest levels of pressure fluctuation at the stator 1 vane passing period on its second 2<sup>nd</sup> harmonic at 1620Hz and 3240Hz, respectively. However, as seen in Fig. 13 Sensor S8 does not exhibit the same type of fluctuating pressure pattern, with a much wider frequency content. When analyzing the frequency spectrum in Fig. 14(b), one can observe two dominant frequencies related to stator 1 and stator 2 vane passing periods at 1620Hz and 2025Hz. These dominant frequencies show however a deficit of 60% and 75% in pressure fluctuations compared to sensor S1 pressure fluctuation at 1620Hz. Due to its location, sensor S8 is affected by the presence of the rotor hub passage vortex migrating from the pressure side to suction side of the adjacent blade across the passage and centered around 20% span. As the rotor travels circumferentially, the radial location of the rotor hub passage vortex is strongly modulated. The first source of radial migration of the hub passage vortex is caused by its interaction with stator 1 hub passage vortex, as found by Behr et al.[15], and is responsible for the peak present at 1620Hz. The second source of periodical fluctuations is caused by the interaction of the rotor passage vortex with stator 2 potential field at 2025Hz, which tends to modulate the intensity and the circumferential position of the hub rotor passage vortex compared to the blade suction side, as reported in [15, 16]. Kai et al. [17] reports a the third cause for the radial migration of the hub passage vortex related to its interaction with the rim seal purge flow, that is triggered by the rotor blade passing period at 2430Hz. This could explain the presence of the fourth largest peak in measured pressure at 4860Hz in Fig. 14(b).

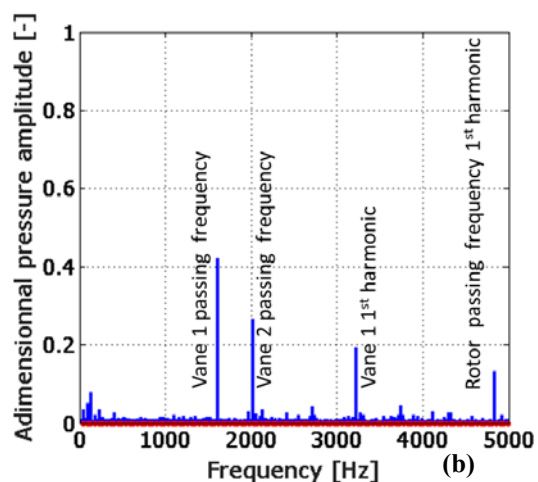
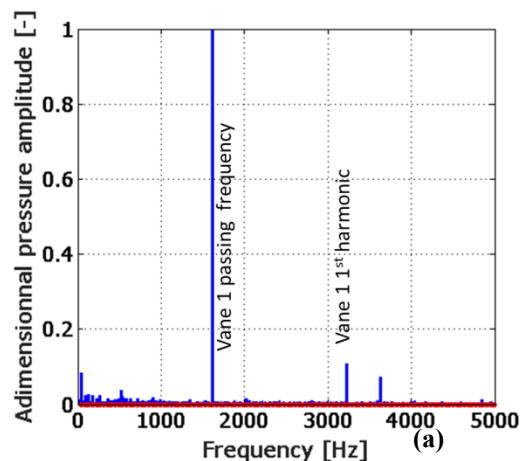


**Fig. 14: (a) Sensor S1 frequency spectrum, (b) Sensor S8 frequency spectrum, both power spectrum are non-dimensionnalized by the maximum pressure amplitude of sensor 1**

### Concluding remarks

A novel multi-sensor wireless measurement system for measurements in the rotating frame of reference  $s$  developed and demonstrated. The system is comprised of in-house surface mount pressure sensors and wireless signal conditioning and acquisition boards.

The surface mount pressure sensors use ultra-miniature absolute pressure sensors packaged into aluminum containers for installation onto stationary vanes or rotating blades. Two surface mount pressure sensor assemblies are developed in the context of this work. The first assembly consists of RTV-coated pressure transducer (SMA-RTV), whereas the second assembly is equipped with a perforated screen to protect the membrane in harsh environment (SMA-PS). Both sensor assemblies have been fully calibrated and characterized. The uncertainty analysis shows that both assemblies offer a similar measurement accuracy of  $\pm 87$ Pa and  $\pm 77$ Pa in absolute and fluctuating pressure measurements, respectively. But, the RTV-coated assembly offers the highest measurement bandwidth of 210 kHz which provides the required measurement bandwidth to resolve the unsteady pressure fluctuations up to more than 40 blade passing period harmonics for most of the existing turbomachines. The sensors and the wireless data acquisition boards provide a high signal-to-noise ratio with pressure resolution of 6Pa on

the raw signal.

The measurement system was successfully deployed and operated in an axial one-and-1/2-stage-turbine facility. The rotor blades were equipped with 32 sensors located on the rotor blades at 20% and 85% span. The measurement system has proven to be able to capture the temporal fluctuations in rotor blade surface pressure related to the inter-blade row interactions, either at the leading edge or at the trailing edge of the rotor blade. It has been shown that the surface pressure fluctuation on the suction side near the trailing edge at 20% span is mainly affected by the periodical radial migration of the rotor hub passage vortex. The migration rotor hub passage vortex being caused mainly by its interaction with stator 1 hub passage vortex, stator 2 potential field and the rim seal purge flow.

### Acknowledgements

The authors would like to acknowledge the support of Prof. Sergiadis in the development of the wireless data acquisition system, as well as the support of Matthias Matter for his help in performing the various sensor calibrations.

### REFERENCES

- [1] R. J. Miller, R. W. Moss, R. W. Ainsworth, and C. K. Horwood, "Time-resolved vane-rotor interaction in a high-pressure turbine stage," *Journal of Turbomachinery-Transactions of the Asme*, vol. 125, pp. 1-13, Jan 2003.
- [2] B. Laumert, H. Martensson, and T. H. Fransson, "Investigation of unsteady aerodynamic blade excitation mechanisms in a transonic turbine stage - Part I: Phenomenological identification and classification," *Journal of Turbomachinery-Transactions of the Asme*, vol. 124, pp. 410-418, Jul 2002.
- [3] B. Adiloglu, G. Paniagua, and T. Yasa, "Unsteady Aerodynamic Blade Forces due to strong Vane Shocks," in *8th International Symposium on Experimental and Computational Aerodynamics of Internal Flows*, Lyon, July, 2007.
- [4] S. König, N. Petry, and N. G. Wagner, "Aeroacoustic Phenomena in High- Pressure Centrifugal Compressors - A Possible Root Cause for Impeller Failures," in *Texas A&M 37th Turbomachinery Symposium, Lecture 9*, 2009.
- [5] A. Kammerer and R. S. Abhari, "Blade Forcing Function and Aerodynamic Work Measurements in a High Speed Centrifugal Compressor With Inlet Distortion," *Journal of Engineering for Gas Turbines and Power-Transactions of the Asme*, vol. 132, SEP 2010.
- [6] S. K. Richards, K. Ramakrishnan, C. M. Shieh, F. Moyroud, A. Picavet, V. Ballarini, and V. Michelassi, "Unsteady Acoustic Forcing on an Impeller Due to Coupled Blade Row Interactions," *Journal of Turbomachinery-Transactions of the Asme*, vol. 134, Nov 2012.
- [7] K. Kupferschmied, P. Köppel, C. Roduner, and G. Gyarmathy, "On The Development and Application of the FRAP (Fast-Response Aerodynamic Probe) System for Turbomachines-Part 1: The Measurement System," *J. Turbomachinery*, vol. 122, pp. 505-516, 2000.
- [8] M. Mansour, N. Chokani, A. I. Kalfas, and R. S. Abhari, "Time-Resolved Entropy Measurements Using a Fast Response Entropy Probe " *Meas. Sci. Technol.*, vol. 10 p. 115401 (14pp), 2008.
- [9] C. Lenherr, A. I. Kalfas, and R. S. Abhari, "High Temperature Fast Response Aerodynamic Probe," *Journal of Engineering for Gas Turbines and Power-Transactions of the ASME*, vol. 133, Jan 2011.
- [10] K. Vogel, A. Zemp, and R. S. Abhari, "Experimental and Numerical Investigation of the Unsteady Flow Field in a Vaned Diffuser of a High-Speed Centrifugal Compressor," Düsseldorf, Germany, 2014.
- [11] B. Rollinger, M. Mansour, and R. S. Abhari, "High temperature fast response pressure probe for use in liquid metal droplet dispensers," *Rev. Sci. Instrum.*, vol. 83, 2012.
- [12] C. Gossweiler, H. J. Humm, and P. Kupefrschmied, "The Use of Piezo-Resistive Semi-Conductor Pressure Transducers for Fast-Response Probe Measurements in Turbomachinery," in *Proc. 10th Symposium on Measuring Techniques for Transonic and Supersonic Flows in Cascades and Turbomachines*, Brussel, 1989.
- [13] T. Behr, A. I. Kalfas, and R. S. Abhari, "A Probabilistic Uncertainty Evaluation Method for Turbomachinery Probe Measurements " in *The XVIIIth Bi-Annual Symposium on Measuring Techniques in Transonic and Supersonic Flows in Cascades and Turbomachines*, Thessaloniki, Greece, 2006.
- [14] P. Rebholz, A. I. Kalfas, and R. S. Abhari, "Low pressure turbine blade forcing amplitude and phase prediction errors," in *Asme Turbo Expo 2016*, to be presented, 2016.
- [15] T. Behr, A. I. Kalfas, and R. S. Abhari, "Unsteady flow physics and performance of a one-and 1/2-stage unshrouded high work turbine," *Journal of Turbomachinery-Transactions of the Asme*, vol. 129, pp. 348-359, Apr 2007.
- [16] M. Mansour, N. Chokani, A. I. Kalfas, and R. S. Abhari, "Impact of Time-Resolved Entropy Measurement on a One-and-One-Half-Stage Axial Turbine Performance," *Journal of Turbomachinery-Transactions of the Asme*, vol. 134, MAR 2012.
- [17] K. Regina, A. I. Kalfas, and R. S. Abhari, "Experimental Investigation of Purge Flow Effects on a High Pressure Turbine Stage," *Journal of Turbomachinery-Transactions of the Asme*, vol. 137, Apr 2015.